

# Ultra-thin nanocrystalline n-type silicon oxide front contact layers for rear-emitter silicon heterojunction solar cells

L. Mazarella<sup>\*,a</sup>, A. B. Morales-Vilches<sup>a</sup>, L. Korte<sup>b</sup>, R. Schlatmann<sup>a</sup> and B. Stannowski<sup>a</sup>

<sup>a</sup>PVcomB, Helmholtz-Zentrum Berlin für Materialien und Energie, Schwarzschildstr. 3, 12489 Berlin, Germany

<sup>b</sup>Institute for Silicon Photovoltaics, Helmholtz-Zentrum Berlin für Materialien und Energie, Kekuléstraße 5, 12489 Berlin, Germany

## Abstract

Hydrogenated nanocrystalline silicon oxide (nc-SiO<sub>x</sub>:H) films have demonstrated a unique combination of low parasitic absorption and high conductivity. Here, we report on the use of n-type nc-SiO<sub>x</sub>:H as front surface field (FSF) in rear-emitter silicon heterojunction (SHJ) solar cells exhibiting excellent electrical cell parameters at a thickness down to only 5 nm. Using a seed layer, we are able to maintain excellent electrical performance (high fill factor (*FF*) and open circuit voltage (*V*<sub>OC</sub>)), while enhancing layer transparency for maximizing short circuit current (*J*<sub>SC</sub>). These results, together with the short deposition time (< 100 s), make the (n)nc-SiO<sub>x</sub>:H FSF attractive for reducing production costs in industrial applications. The best device, with the optimized (n)nc-SiO<sub>x</sub>:H FSF layer, shows *V*<sub>OC</sub> of 731 mV, *FF* of 80.6%, *J*<sub>SC</sub> of 38.3 mA/cm<sup>2</sup> and a power conversion efficiency of 22.6%.

**Keywords:** Nanocrystalline silicon oxide, Optical simulations, Silicon, Silicon heterojunction (SHJ) solar cells.

\*Corresponding author: e-mail: luana.mazarella@helmholtz-berlin.de, Phone: +49-30-8062-15043, Fax: +49-30-8062-15677.

## 1. Introduction

Silicon heterojunction (SHJ) solar cells are attractive due to their high efficiency potential combined with a lean and cost-effective production process featuring only four main process steps. In SHJ cells with contacts on both sides of the c-Si wafer hydrogenated amorphous silicon (a-Si:H) i/n and i/p layer stacks, grown by plasma-enhanced chemical vapor deposition (PECVD), commonly form the passivated contacts for electrons and holes, respectively. These passivated contacts result in the highest reported open circuit voltages (*V*<sub>OC</sub>) for silicon solar cells, of 750 mV [1]. Transparent conducting oxide (TCO) layers are needed to laterally collect the charge carriers to the metal grid. The main efficiency limitation in this cell type is due to parasitic light absorption in the front contact formed by the silicon layer stack together with the TCO and shading losses in the metal grid. Even though a two-side contacted SHJ solar cell with an efficiency of 25.1% and a short circuit current density (*J*<sub>SC</sub>) of 40.8 mA/cm<sup>2</sup> were reported by Kaneka [2], this cell is still limited by parasitic absorption losses. This is evidenced by the substantial *J*<sub>SC</sub> difference as compared to all-back-contacted SHJ cells: Kaneka recently reached 26.6% and *J*<sub>SC</sub> as high as 42.5 mA/cm<sup>2</sup> with the back-contacted SHJ [3]. Traditionally, in SHJ cells the p-type emitter has been at the front side for collecting the minorities on the illuminated side and, thereby, achieving shortest average minority charge carrier diffusion paths. The high quality of today's CZ-Si wafers with minority carrier life times of several milliseconds offer the possibility to apply the p-type emitter on the rear side without increased collection losses. This rear-emitter SHJ cell concept opens new

options for more transparent front stacks, and also relaxes the requirements of the front TCO, which is interesting for industrial production as discussed by Bivour *et al.* [4].

In a recent publication we discussed the role of thickness and refractive index of n-type nanocrystalline silicon oxide (nc-SiO<sub>x</sub>:H) front contacts replacing the a-Si:H n layer on textured and flat SHJ cells [5]. This material, with doped silicon crystallites embedded in an amorphous silicon oxide matrix, had been originally developed for thin film silicon solar cells, such as a-Si:H/μc-Si:H (“micromorph”) tandems cells, for example acting as intermediate reflecting layer [6], and, finally, replacing all doped silicon layers. The nanostructure of this highly heterogeneous and anisotropic material is described in [7,8]. The PECVD growth process, which uses a high hydrogen dilution of the silane gas combined with high plasma power and adding CO<sub>2</sub> to the process gas, was studied by Gabriel *et al.* [9].

Here, we introduce ultra-thin (n)nc-SiO<sub>x</sub>:H front contacts for high efficiency SHJ cells. The challenge of applying nc-SiO<sub>x</sub>:H contacts in SHJ solar cells is to grow highly crystalline and very thin layers on top of the amorphous passivation layer without deteriorating the passivation. A *thin* layer with short deposition time (~ 100 s) is, moreover, mandatory to keep production costs low. It requires prompt nucleation of crystal growth, which is challenging due to the inherent growth properties of nc-Si:H films, with crystalline growth generally starting only after a certain (amorphous) incubation phase [10]. A large flux of atomic hydrogen towards the substrate in a high-pressure-high-power PECVD regime together with a seed layer are required to promote fast transition from

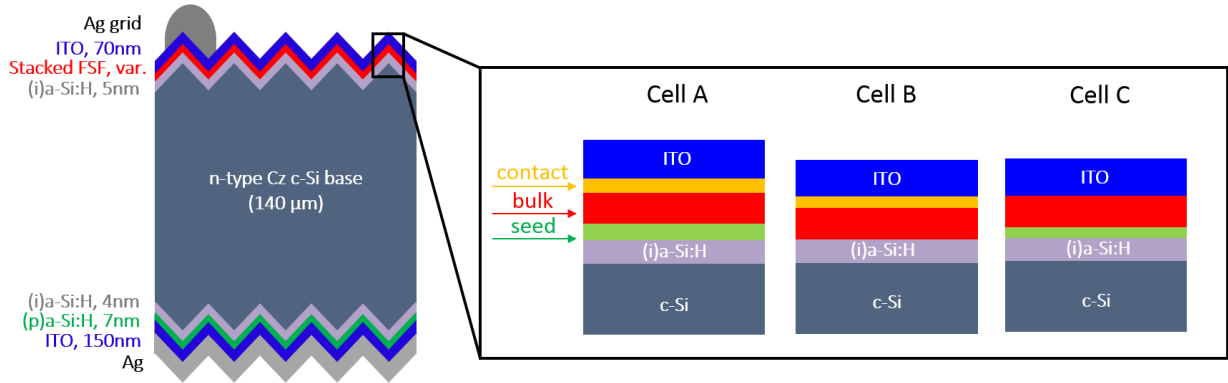


**Figure 1** (left) Cross sectional sketch of a textured SHJ solar cell in rear emitter configuration. The nominal thickness is reported for each layer. (right) Three different front surface field (FSF) stacks as investigated in the present paper on textured c-Si wafers: cell A with nc-Si:H seed- and contact layers; cell B without seed but including the contact layer; and cell C with seed, but without contact layer. Seed and contact are non-oxidic (n)nc-Si:H films while the bulk is an (n)nc-SiO<sub>x</sub>:H film, variable in thickness. The layers are not to scale.

amorphous to nanocrystalline growth and, thereby, control the film nanostructure [11–14]. Additionally, we have shown in our previous study that the surface passivation quality can be even enhanced due to these nc-Si:H-specific PECVD growth conditions, replacing the hydrogen plasma treatment that is usually combined with (i)a-Si:H layer to passivate dangling bonds with H [15]. This feature further reduces the overall deposition time of the (i)/(n) stack as compared to the usually used amorphous stack.

The challenge of controlling optoelectronic properties of nc-SiO<sub>x</sub>:H and combining both highest fill factor ( $FF$ ) and high open circuit voltage ( $V_{OC}$ ) in SHJ solar cells has not yet been completely solved. Various techniques have been suggested to accelerate the nucleation of crystallites and facilitate the integration on ultra-thin nanocrystalline Si films in SHJ cells. Among them are: higher plasma frequencies [16], a layer-by-layer growth technique [10], SiF<sub>4</sub> as silicon precursor and eventually addition of Ar to the gas mixture [17], CO<sub>2</sub> [15,18] or H<sub>2</sub> [19,20] plasma treated (i)a-Si:H, or depositing an nc-Si:H seed layer before the nanocrystalline film [21].

In this contribution, we report on thin (n)nc-SiO<sub>x</sub>:H contacts with a low refractive index of 2.7 at 632 nm (indicative of high oxygen content) and high crystalline fraction and electrical conductivity. After evaluating the current losses by optical simulations, strategies to minimize the layer thickness using a seed layer are shown, resulting in SHJ cells with efficiencies above 22.5%.

## 2. Materials and methods

Nanocrystalline silicon (nc-Si:H) and silicon oxide (nc-SiO<sub>x</sub>:H) films were deposited by PECVD at 13.56 MHz plasma excitation frequency in an Applied Materials AKT1600 cluster tool (electrode area 2000 cm<sup>2</sup>) using

SiH<sub>4</sub>, H<sub>2</sub>, PH<sub>3</sub> and CO<sub>2</sub> as process gases. For optical and electrical characterizations, films were deposited with a thickness of 200 nm on glass substrates. Reflection and transmission spectra were fitted using the Tauc-Lorentz dispersion model to obtain the layer thickness, refractive index ( $n$ ) and extinction coefficient ( $k$ ). The film conductivity was measured in the dark and at room temperature by means of two parallel mercury electrodes. Raman scattering spectroscopy allows to quantify the fraction of crystallites (crystalline volume fraction  $F_C$ ) by comparing amorphous and c-Si peaks as discussed in [8].

For solar cell preparation, we used n-type Czochralski (CZ) silicon wafers (c-Si) with a thickness of 140 μm (after texturing) and a resistivity of 5 Ω·cm. The as-cut c-Si substrates were processed to remove the saw damage due to the wafering procedure. Then, the surfaces were chemically textured to obtain random pyramids with a height of about 4 μm and <111> oriented facets [22]. Prior to the PECVD processes, the wafers were cleaned by the RCA procedure [23] and dipped in 1% HF solution for three minutes to etch the native oxide. The rear-emitter cell structure is depicted in Figure 1. The further fabrication process consists of growing, consecutively, the ~5 nm thick (i)a-Si:H passivation layer and the doped contact layers. More details can be found elsewhere [15]. A stacked FSF composed of seed + bulk + contact layers is consecutively grown in the same deposition chamber. Both seed and contact layers consist of n-doped nc-Si:H, i.e. non-oxidic films deposited without CO<sub>2</sub> to enhance nucleation and, thereby, increase the crystallinity fraction of the subsequent thin (n)nc-SiO<sub>x</sub>:H layer (seed) and increase conductivity and reduce contact resistance to the TCO (contact). The estimated thickness for the seed and contact layers are kept constant at ~30 s and 20 s,

respectively. We investigated the role of each layer exploring three FSF structures as sketched in Figure 1. Quasi-steady-state photoconductance lifetime measurements (QSSPC, Sinton Instruments WCT – 120) are performed on cell precursors [(n)/(i)/c-Si/(i)/(p)] after growing the silicon thin films on both sides of the c-Si substrate, and values for the implied  $V_{OC}$  ( $iV_{OC}$ ) and the implied  $FF$  ( $iFF$ ) are calculated. The devices are completed with  $In_2O_3:Sn$  (ITO) layers DC sputtered at room temperature with a thickness of 70 nm (optimized for low optical reflection) on the illuminated side and 150 nm on the rear of the cell. Finally, a full area Ag (400 nm) layer is sputtered on the back and a metal grid is screen printed on the front side. The grid design is optimized to reduce the shadowing down to  $\sim 4\%$ . The cell area of  $4\text{ cm}^2$  is defined by means of aligned TCO sputtering masks on both sides to define 14 cells per wafer. For reference we processed cells with 12 nm thick (n)nc-Si:H FSF, exhibiting the best performance in our SHJ “baseline process”.  $J-V$  characteristics are measured under standard test conditions ( $25^\circ\text{C}$ , dual light source sun simulator, class AAA+) through  $4\text{ cm}^2$  shadow masks. Furthermore, dedicated test cells without grid are included in the layout for measuring external quantum efficiency (EQE) and absorbance ( $1-R$ ). Illumination dependent open circuit voltage (SunsVoc) curves are measured on completed cells using a Sinton Instruments WCT – 120 set up to extract the pseudo-cell parameters, including the pseudo-fill factor (pFF). Transmission electron microscopy (TEM) is performed with a TITAN 80-300 Berlin Holography Special TEM (FEI-Company) operating at an acceleration voltage of 300 kV. The cross sectional lamella was thinned via an Ar-ions (Fischione Ionmill Model 1010). Optical simulations were carried out using the MATLAB-based 1-D program GenPro4 [24] with  $n$  and  $k$  data experimentally extracted as described above to obtain absorption profiles for each layer shown in Figure 1. The current densities equivalent to the respective absorption spectra are calculated by multiplying the simulated absorption with the AM1.5G spectrum and integrating over the spectral region of interest (300 – 1200 nm). The current densities represent losses due to parasitic absorptions for all the layers except for the c-Si base. Carrier collection from other layers, such as the (i)a-Si:H, or any collection losses in the c-Si absorber are not considered.

### 3. Results and discussion

The electrical and optical properties of (n)nc-SiO<sub>x</sub>:H layers grown by PECVD with variable gas mixtures were discussed in Ref. [5]. Here we implement the optimized (n)nc-SiO<sub>x</sub>:H material that exhibited a relatively low

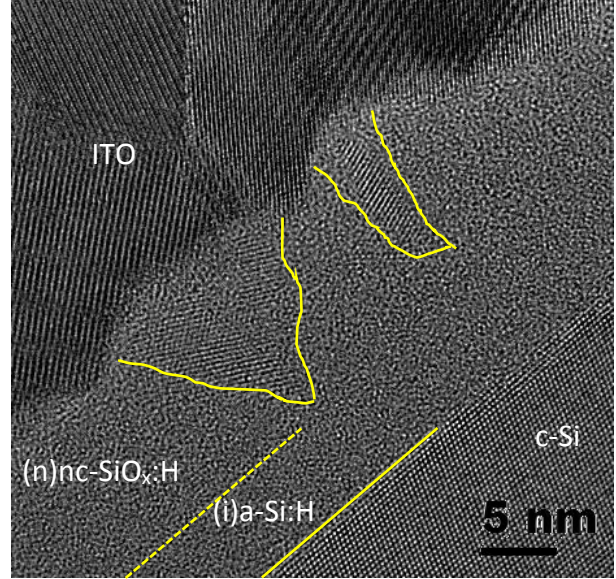


**Figure 2** Cross-sectional TEM micrograph of the front side cell stack (ITO/(n)nc-SiO<sub>x</sub>:H/(i)a-Si:H/c-Si) of cell C (Figure 1). The zone axis orientation for the Si substrate is  $\langle 101 \rangle$ . Yellow lines highlight the boundaries of the passivation layer + incubation phase and curves individual crystals.

refractive index, a high  $F_C$  and electrical conductivity ( $\sigma$ ). For such material grown with  $PH_3/SiH_4$  and  $CO_2/SiH_4$  ratios of 1.6 and 1.2, respectively, we measured on 200 nm thick layers a crystalline volume fraction  $F_C$  of 49%,  $\sigma$  of 0.8 S/cm,  $n$  of 2.7 at 632 nm. The structural properties of this nc-SiO<sub>x</sub>:H layer were further investigated by TEM. Figure 2 shows the cross sectional view of the c-Si/(i)/FSF/ITO stack of cell type C (Figure 1). The micrograph confirms that the (n)nc-SiO<sub>x</sub>:H layer has an anisotropic structure with columnar grains that evolve from the amorphous passivation layer. The latter appears to be slightly thicker than the targeted 5 nm (Figure 1), probably due to the non-oxidic seed and incubation stage of the nanocrystalline layer that are not properly distinguishable from the i-layer. Furthermore, we can confirm that the (n)nc-SiO<sub>x</sub>:H exhibits a substantial nanocrystalline fraction even for a 5 nm thick layer.

#### 3.1 Optical simulations

For the present work we simulated the cell stack for the cell architecture in Figure 1 using GenPro4. As previously demonstrated on textured wafers, parasitic absorption is the dominating loss mechanism, as compared to the reflection fraction [5]. Therefore, a FSF layer with high transparency and reduced thickness, such as nc-SiO<sub>x</sub>:H, is preferred as FSF to minimize absorption losses. Figure 3 shows the absorption profiles of the different layers placed on the front/rear side of the wafers and the reflection out of the cell. In the reference device, the 12 nm nc-Si:H FSF layer causes a parasitic absorption that corresponds to a

current density loss above  $1 \text{ mA/cm}^2$  (yellow area in Figure 3 (a)). The use of a (n)nc-SiO<sub>x</sub>:H with the same thickness reduced parasitic absorption by 60% with a current loss of only  $0.4 \text{ mA/cm}^2$  (red area in Figure 3 (b)). By lowering further the (n)nc-SiO<sub>x</sub>:H layer thickness down to 5 nm the simulated parasitic absorption in the doped layer is reduced to less than  $0.2 \text{ mA/cm}^2$  (not shown here). For the thinnest (n)nc-SiO<sub>x</sub>:H layer a simulated current density of  $40.3 \text{ mA/cm}^2$  is predicted, i.e. a gain of  $0.8 \text{ mA/cm}^2$  as compared to the optimized non-oxidic layer. A high current density is still lost in the (i)a-Si:H layer ( $\sim 0.8 \text{ mA/cm}^2$ ). However, it can be assumed that a fraction of  $\sim 30\%$  of the photogenerated carriers from this film can contribute to the external photocurrent [25]. We emphasize that the simulations depicted in Figure 3 (b) might deviate from the experiments as for example seed or contact layers are not included. Moreover, the  $n$  and  $k$  values were extracted from *thick* layers on glass which most likely have properties deviating from those of the *thin* layers in the cell. The parasitic absorption in the Ag is underestimated as, e.g., absorption due to surface-plasmons [26] is not included in the optical model.

### 3.2 Solar cells

Three sets of samples were prepared with identical processes except for the FSF variations as depicted in Figure 1, denoted as cell types A, B and C. Furthermore, the (n)nc-SiO<sub>x</sub>:H bulk layer was reduced in thickness for cell A.

Table 1 summarizes the cell parameters as an average of 14 cells for each cell type, showing the good homogeneity of our optimized PECVD process for nc-SiO<sub>x</sub>:H. These results demonstrate that excellent electrical cell parameters are possible by using (n)nc-SiO<sub>x</sub>:H, with  $V_{OC} > 730 \text{ mV}$  and  $FF > 80\%$ . The highest conversion efficiency was obtained for the device type C having a seed layer and a 10 nm thick nc-SiO<sub>x</sub>:H without contact layer ( $\eta = 22.4 \pm 0.2\%$ ). Note, that the (n)nc-SiO<sub>x</sub>:H bulk layer can be reduced in thickness with no detrimental effect on any electrical parameters. Our results are in contrast with previous reports [27,28] where  $V_{OC}$  and  $FF$  degradations are measured already for a nc-SiO<sub>x</sub>:H layer below 20 nm.

The parameters of the best cell of each cell type are plotted in Figure 4. In order to illuminate the cause for differences in electrical performance, carrier lifetime curves (QSSPC) measured on all cell precursors prior to TCO sputtering are analyzed (Figure 5). The implied open circuit voltages ( $i$ - $V_{OC}$ s) extracted from these measurements are also shown in Figure 4 (a). Besides the  $FF$  taken from the  $J$ - $V$  characteristics, also implied  $FF$  ( $i$ - $FF$ ) values extracted from Figure 5 and pseudo- $FF$ s ( $p$ - $FF$ ) from  $SunsV_{OC}$  are added for comparison. The latter can be

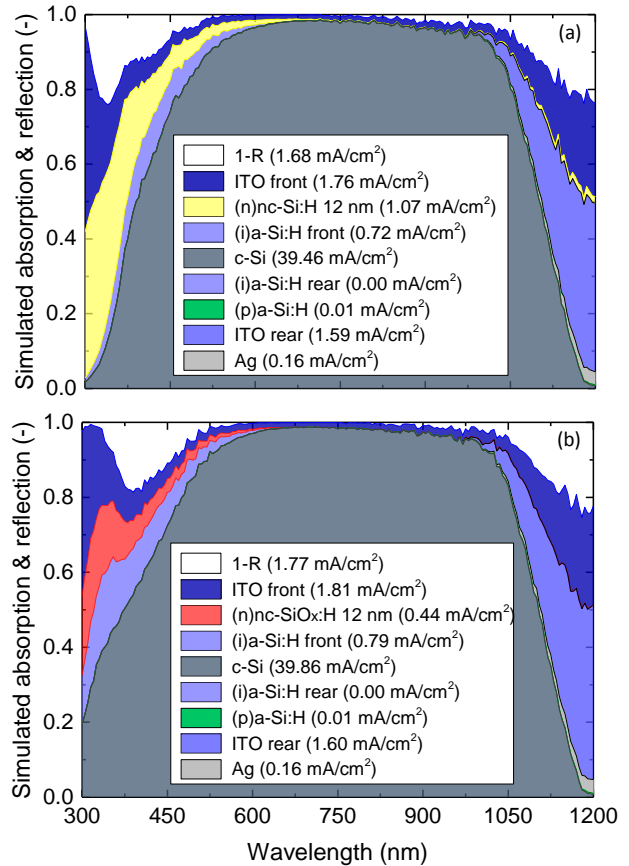


**Figure 3** Simulated absorption and reflection profiles for a SHJ solar cells with 12 nm (a) (n)nc-Si:H (reference) and (b) (n)nc-SiO<sub>x</sub>:H FSF layer. For each layer, the corresponding calculated current density is given. The thickness of the other layers are specified in Figure 1. The front ITO thickness is increased by 10% for the reference cell.

interpreted as the potential upper limit for the solar cell's  $FF$  and comparing it to the  $FF$  from  $J$ - $V$  gives indirect evidence of series resistance losses.

Comparing the cells of type A, B and C with 10 nm bulk (n)nc-SiO<sub>x</sub>:H layers evidences the high electrical quality of the (n)nc-SiO<sub>x</sub>:H material: for all the variations we have tested (cf. Figure 1), the cell performance stays on a very good level. The results obtained for cell A and B with 10 nm FSF indicate that the presence of a highly crystalline and non-oxidic nc-Si:H seed layer increases both  $V_{OC}$  and  $FF$ . We can deduce that a clear effect of the seed layer on the nanocrystalline silicon growth is observed for the FSF. In particular, cell type B exhibits lower performances, specifically a lower open circuit voltage is measured with  $V_{OC}$  of 725 mV, while the cells with the seed exhibited  $V_{OC}$ s of 730 mV (cell A and C). Comparing the QSSPC curves in Figure 5 (a) we can observe a different shape in the low injection range (below  $10^{15} \text{ cm}^{-3}$ ). Usually, changes at low injection levels are related to changes in the internal electric field created by

the doped layers [15,29]: At the nc-Si:H (or a-Si:H)/c-Si heterojunction, strong fields reduce the Shockley-Read-Hall recombination [30] due to a strong depletion of one carrier type. This is the so-called field-effect passivation. In Figure 5(a), the shape of curve B clearly indicates a lower field-effect passivation as compared to the cells A

and C, with a negative effect on both  $i-V_{OC}$  and  $i-FF$ . Both cell types with seed exhibit a  $i-V_{OC}$  of 735 mV and effective minority carrier lifetimes ( $\tau_{eff}$ ) > 3 ms measured at injection level of  $10^{16}$  and  $10^{15}$  cm, respectively. Growing the (n)nc-SiO<sub>x</sub>:H *without* seed (cell B) results in clearly lower  $\tau_{eff}$  of 1.3 ms and  $i-V_{OC}$  of 727 mV.

**Table 1** Cell parameters of devices with reference nc-Si:H FSF and cell type A, B and C. The values reported are the average based on 14 cells on the same wafer and the best cell in brackets. The standard deviation is calculated for each cell parameter.

Cell type	FSF bulk (nm)	$V_{OC}$ (mV)	$J_{SC}$ (mA/cm <sup>2</sup> )	$FF$ (%)	$\eta$ (%)
nc-Si:H Ref.	12	725.2 ± 3.7 (728.9)	37.7 ± 0.1 (37.8)	79.0 ± 1.4 (79.7)	21.4 ± 0.5 (21.9)
nc-SiO <sub>x</sub> :H_A	5	729.7 ± 1.2 (730.6)	38.3 ± 0.1 (38.3)	79.9 ± 0.3 (80.3)	22.3 ± 0.2 (22.5)
	7.5	728.7 ± 1.6 (730.4)	38.3 ± 0.1 (38.4)	79.2 ± 0.9 (79.9)	22.1 ± 0.3 (22.4)
	10	728.7 ± 1.6 (729.4)	38.3 ± 0.1 (38.3)	78.9 ± 0.6 (79.6)	22.0 ± 0.2 (22.3)
nc-SiO <sub>x</sub> :H_B	10	724.2 ± 1.0 (724.8)	38.8 ± 0.1 (38.8)	77.7 ± 0.5 (78.3)	21.8 ± 0.2 (22.1)
nc-SiO <sub>x</sub> :H_C	10	729.5 ± 1.2 (730.7)	38.4 ± 0.1 (38.3)	80.0 ± 0.4 (80.6)	22.4 ± 0.2 (22.6)

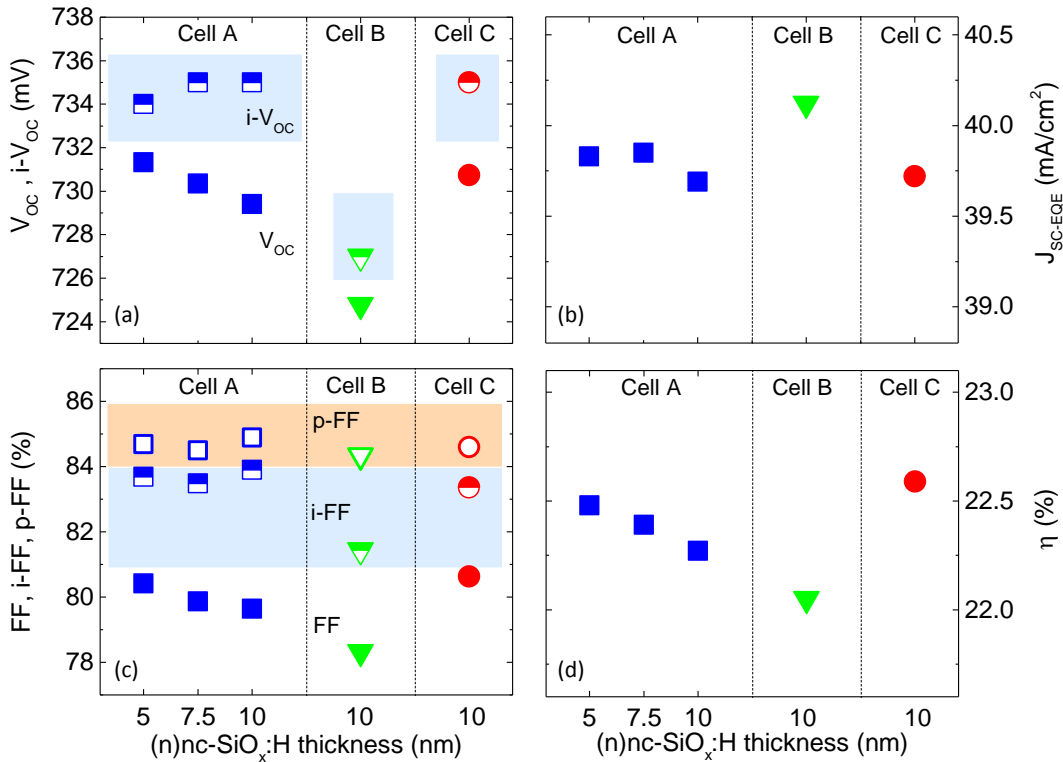


**Figure 4** Best cell parameters of SHJ cells vs. (n)nc-SiO<sub>x</sub>:H thickness for cell structures with seed- and contact layers (cell A), without seed (cell B) and with seed, but without contact layer (cell C). (a) Open circuit voltage based on the  $J-V$  curve ( $V_{OC}$ ) and implied ( $i-V_{OC}$ ) from QSSPC, (b) short circuit current from EQE ( $J_{SC-EQE}$ ), (c) fill factor derived by different methods ( $FF$ ,  $i-FF$  and  $p-FF$ ) and (d) conversion efficiency  $\eta$  (based on the  $J-V$  measured  $J_{SC}$ ). The cell structures are depicted in Figure 1.

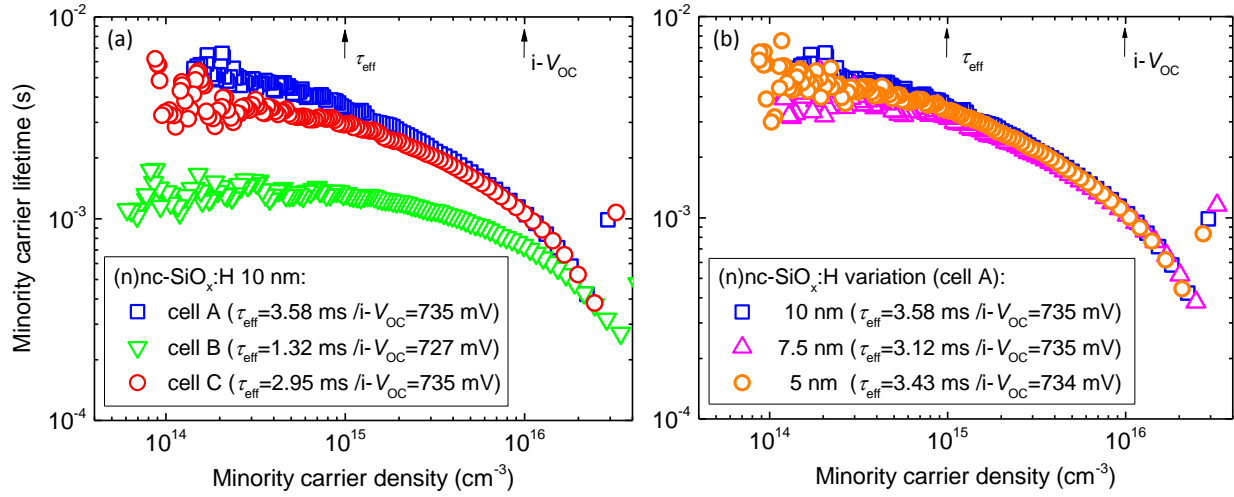


**Figure 5** Minority carrier lifetime measurements performed on cell precursors deposited on textured c-Si wafers. (a) Samples with cell A structure and variable (n)nc-SiO<sub>x</sub>:H bulk layer thickness (range 10 – 5 nm). (b) Samples with 10 nm thick (n)nc-SiO<sub>x</sub>:H bulk layer with both seed and contact (cell A), without seed (cell B) and without contact (cell C).  $\tau_{\text{eff}}$  and  $i\text{-}V_{\text{OC}}$  are extracted at minority carrier density of  $10^{15}$  and  $10^{16}$  cm<sup>-3</sup>, respectively. The sketch of the cell structures are depicted in Figure 1.

Further indication of the poorer electrical properties is the lower  $FF$  measured for cell B (78.3%) with approximately 2.3% absolute losses, as compared to cell type A processed instead with the full FSF stack (Figure 4 (c)). It can be seen that there is only a small difference in  $p\text{-}FF$  among the three cell types with values in the range 84 – 85%. The  $i\text{-}FF$  of cell A and C are on the same level and only slightly lower than the  $p\text{-}FF$  ones. On the contrary, cell B shows a considerably lower  $i\text{-}FF$ . A similar trend is observed in  $FF$  values from  $J\text{-}V$  characteristics as discussed above. We can conclude from this analysis that the difference in  $p\text{-}FF$  for all cell types as compared to the  $FF$  (and  $i\text{-}FF$ ) can be attributed to series resistance losses. Moreover, cell B exhibits a larger difference that confirms once more the key role of the seed for prompt nanocrystalline growth. The trends discussed for  $i\text{-}V_{\text{OC}}$  and  $i\text{-}FF$  are consistent with the  $V_{\text{OC}}$  and  $FF$  trends as shown in Figure 4. This observation supports our hypothesis on the role of the seed in accelerating the nanocrystalline growth and leading to higher dopant activation, thus a more pronounced field effect. In fact, the deposition conditions for the seed layer (namely  $\text{H}_2/\text{SiH}_4$  ratio, pressure and power) are very similar to the (n)nc-SiO<sub>x</sub>:H bulk ones. Consequently, both the lower  $V_{\text{OC}}$  (– 4.6 mV) and  $FF$  limit the conversion efficiency of cell type B at 22%, while  $\eta = 22.3\%$  is obtained after introducing the seed layer in cell C, fabricated without the contact layer. This cell exhibits the highest  $FF$  of 80.6%.

Moreover, looking at values reported in Figure 4 (b), cell B exhibits a short current density calculated from EQE ( $J_{\text{SC-EQE}}$ ) of 40.1 mA/cm<sup>2</sup> with a gain of 0.4 mA/cm<sup>2</sup> in the

short wavelength range (< 600 nm) as compared to the cells with a seed (cell A and C) in Figure 6. This might be explained, by both removal of the nc-Si:H seed that is more parasitically absorptive than nc-SiO<sub>x</sub>:H and by the delayed nucleation, hence, a larger a-SiO<sub>x</sub> (reduced nc-Si:H) fraction.

Finally, the reduction of the (n)nc-SiO<sub>x</sub>:H thickness down to 5 nm (cell A) has no significant effect on the minority carrier lifetime curves as shown in Figure 5 (b) with a constant  $i\text{-}V_{\text{OC}}$ . The field-effect passivation does not depend on the FSF thickness for our specific (n)nc-SiO<sub>x</sub>:H

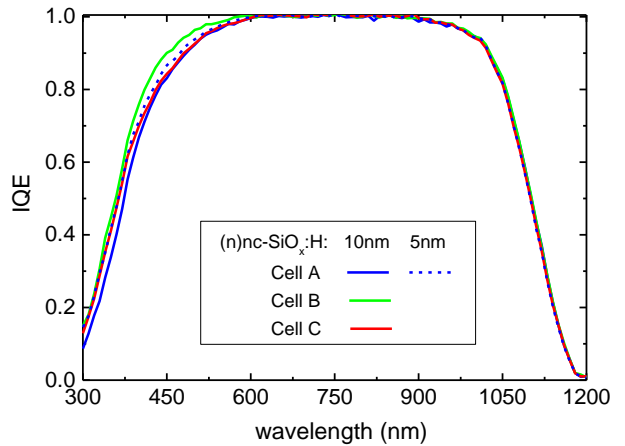


**Figure 6** Internal quantum efficiency calculated from the  $1\text{-}R$  and EQE spectra (not shown here) as a function of wavelength. for the best cells shown in Figure 4 with 10 nm (n)nc-SiO<sub>x</sub>:H bulk layer and different configurations (cell type A, B and C). The dotted curve represent the cell type A with a reduced (n)nc-SiO<sub>x</sub>:H thickness of 5 nm.

layer. This indicates that if the growth is enhanced by the seed layer, the (n)nc-SiO<sub>x</sub>:H layer develops a sufficient conductivity to provide a low contact resistance to the front ITO and the additional contact layer is not needed. We also observe that the reduction of (n)nc-SiO<sub>x</sub>:H thickness yields an increase in  $V_{OC}$  with the highest value of 730.6 mV for the thinnest bulk layer. The  $FF$  follows the same trend with a maximum of 80.3% and, moreover, the  $p$ - $FF$  stays on the same level as experimented for the thicker nc-SiO<sub>x</sub>:H FSF layers. This is consistent with our finding that both the high  $FF$  values (Figure 4) and the field-effect passivation (Figure 5) remain unaffected by the thickness reduction. The thinner (n)nc-SiO<sub>x</sub>:H leads to a small gain in  $J_{SC-EQE}$ . The reduced parasitic absorption is detectable in the IQE curves, with a slightly higher spectral response at 400–600 nm for the thinnest FSF layer (Figure 6). Consequently, the gains in  $J_{SC-EQE}$  and  $FF$  lead to a conversion efficiency of 22.5% for the thinnest FSF, i.e. about 1% relative improvement as compared to cell A with 10 nm (n)nc-SiO<sub>x</sub>:H.

Finally, to demonstrate scalability, we prepared solar cells on full-area CZ c-Si wafers (total area 244.35 cm<sup>2</sup>) applying the 10 nm (n)nc-SiO<sub>x</sub>:H FSF of cell type C. Without any further optimization of film properties for the larger cell size, we measure comparable current density, but slightly lower electrical parameters as compared to the average values reported in Table 1 ( $FF$  – 2.5% absolute and  $V_{OC}$  –9 mV). We attribute this to handling and wafer-edge effects that are less detrimental for the masked 4 cm<sup>2</sup> cells. The best full-size cell shows  $J_{SC}$  of 38.4 mA/cm<sup>2</sup>,  $V_{OC}$  of 720.2 mV,  $FF$  of 77.5% with  $\eta$  = 21.4%.

#### 4. Conclusion

We have studied PECVD-grown (n)nc-SiO<sub>x</sub>:H layers that exhibit both excellent optical and electrical properties with relevance for application as front surface field (FSF) in rear-emitter silicon heterojunction (SHJ) solar cells. In particular, the high transparency of these films and their reduced thickness strongly reduce parasitic absorption in the low wavelength range, enhancing the photocurrent density. TEM micrographs confirm the layer thicknesses and the presence of nanocrystals in thin (n)nc-SiO<sub>x</sub>:H layers grown on the amorphous passivation layer. Optical simulations indicate a potential gain in  $J_{SC}$  of 0.8 mA/cm<sup>2</sup> by using an extremely thin (n)nc-SiO<sub>x</sub>:H film, as compared to the optimized, non-oxidic reference nc-Si:H layer. A reduction in parasitic absorption by 85% for this thin FSF is estimated, where less than 0.2 mA/cm<sup>2</sup> are lost within the 5 nm nc-SiO<sub>x</sub>:H layer.

Applying the optimized (n)nc-SiO<sub>x</sub>:H layer in SHJ cells, we have shown devices with both high fill factor ( $FF$ ) and open circuit voltage ( $V_{OC}$ ). High homogeneity

and reproducibility of all cell parameters indicate a stable PECVD deposition process for (n)nc-SiO<sub>x</sub>:H growth, also shown on a industrially relevant wafer size of 244 cm<sup>2</sup>. We have discussed the important role of a non-oxidic seed layer on the nanocrystalline evolution, as evidenced by analyzing solar cell parameters and carrier lifetime curves. We deduce, therefore, that the lack of a nanocrystalline seed is detrimental for  $V_{OC}$  and  $FF$ , which can be explained by the poor nc-SiO<sub>x</sub>:H nucleation. The best cell reached  $V_{OC}$  of 731 mV,  $FF$  of 80.6%,  $J_{SC}$  of 38.3 mA/cm<sup>2</sup> ( $J_{EQE-SC}$  = 39.7 mA/cm<sup>2</sup>) and  $\eta$  of 22.6%.

Furthermore, a remarkably high  $\eta$  of 22.5% are reported for a (n)nc-SiO<sub>x</sub>:H layer of only 5 nm with a total deposition time of 95 s that makes this layer attractive for low-cost production. These results indicate that the material has a sufficient high conductivity (and doping) to not negatively influence the band banding at the (n)nc-SiO<sub>x</sub>:H/(n)FSF side even for such ultra-thin (n)nc-SiO<sub>x</sub>:H FSF layer.

#### Acknowledgements

The authors thank Dr. Martin Ledinsky (Institute of Physics, Academy of Sciences of the Czech Republic) for Raman measurements and for fruitful discussions. Furthermore, we thank K. Bhatti, D. Debrassine, A. Cruz Bournazou, M. Hartig, T. Hänel, K. Jacob, S. Kolb, K. Mack, H. Rhein and M. Werth for technical support. We gratefully acknowledge the financial support by the German Federal Ministry of Economic Affairs and Energy within the project HERA (reference #03258251). Parts of this work were supported by the European Union's Horizon 2020 Programme for research, technological development and demonstration under grant agreement no. 727523 (project NextBase).

#### References

- [1] M. Taguchi, A. Yano, S. Tohoda, K. Matsuyama, Y. Nakamura, T. Nishiwaki, K. Fujita and E. Maruyama, "24.7% Record Efficiency HIT Solar Cell on Thin Silicon Wafer", *IEEE Journal of Photovoltaics*, 4 (2014) 96–99.
- [2] D. Adachi, J. Hernández and K. Yamamoto, "Impact of carrier recombination on fill factor for large area heterojunction crystalline silicon solar cell with 25.1% efficiency", *Applied Physics Letters*, 107 (2015) 233506.
- [3] K. Yoshikawa, H. Kawasaki, W. Yoshida, T. Irie, K. Konishi, K. Nakano, T. Uto, D. Adachi, M. Kanematsu, H. Uzu and K. Yamamoto, "Silicon heterojunction solar cell with interdigitated back contacts for a photoconversion efficiency over 26%", *Nature Energy*, 2 (2017) 17032.
- [4] M. Bivour, H. Steinkemper, J. Jeurink, S. Schröer and M. Hermle, "Rear Emitter Silicon Heterojunction Solar Cells: Fewer Restrictions on the Optoelectrical Properties of Front Side TCOs", *Energy Procedia*, 55 (2014) 229–234.

- [5] L. Mazzarella, A. Morales-Vilches, M. Hendrichs, S. Kirner, L. Korte, R. Schlatmann and B. Stannowski, "Nanocrystalline n-Type Silicon Oxide Front Contacts for Silicon Heterojunction Solar Cells: Photocurrent Enhancement on Planar and Textured Substrates", *IEEE Journal of Photovoltaics*, (2017) accepted, under publication.
- [6] S. Kirner, S. Calnan, O. Gabriel, S. Neubert, M. Zelt, B. Stannowski, B. Rech and R. Schlatmann, "An improved silicon-oxide-based intermediate-reflector for micromorph solar cells", *physica status solidi C*, 9 (2012) 2145–2148.
- [7] P. Cuony, D. Alexander, I. Perez-Wurfl, M. Despeisse, G. Bugnon, M. Boccard, T. Söderström, A. Hessler-Wyser, C. Hébert and C. Ballif, "Silicon Filaments in Silicon Oxide for Next-Generation Photovoltaics", *Advanced Materials*, 24 (2012) 1182–1186.
- [8] M. Klingsporn, S. Kirner, C. Villringer, D. Abou-Ras, I. Costina, M. Lehmann and B. Stannowski, "Resolving the nanostructure of plasma-enhanced chemical vapor deposited nanocrystalline SiO<sub>x</sub> layers for application in solar cells", *Journal of Applied Physics*, 119 (2016) 223104.
- [9] O. Gabriel, S. Kirner, M. Klingsporn, F. Friedrich, B. Stannowski and R. Schlatmann, "On the Plasma Chemistry During Plasma Enhanced Chemical Vapor Deposition of Microcrystalline Silicon Oxides", *Plasma Processes and Polymers*, 12 (2015) 82–91.
- [10] P. Roca i Cabarrocas, N. Layadi, T. Heitz, B. Drévillon and I. Solomon, "Substrate selectivity in the formation of microcrystalline silicon: Mechanisms and technological consequences", *Applied Physics Letters*, 66 (1995) 3609.
- [11] P. Roca i Cabarrocas, A. Fontcuberta i Morral, B. Kalache and S. Kasouit, "Microcrystalline Silicon Thin-Films Grown by Plasma Enhanced Chemical Vapour Deposition - Growth Mechanisms and Grain Size Control", *Solid State Phenomena*, 93 (2003) 257–268.
- [12] P. Roca i Cabarrocas, "New approaches for the production of nano-, micro-, and polycrystalline silicon thin films", *physica status solidi C*, 1 (2004) 1115–1130.
- [13] A. Matsuda, "Growth mechanism of microcrystalline silicon obtained from reactive plasmas", *Thin Solid Films*, 337 (1999) 1–6.
- [14] S. Sriraman, S. Agarwal, E. Aydil and D. Maroudas, "Mechanism of hydrogen-induced crystallization of amorphous silicon", *Nature*, 418 (2002) 62–65.
- [15] L. Mazzarella, S. Kirner, O. Gabriel, S. Schmidt, L. Korte, B. Stannowski, B. Rech and R. Schlatmann, "Nanocrystalline silicon emitter optimization for Si-HJ solar cells: Substrate selectivity and CO<sub>2</sub> plasma treatment effect", *physica status solidi A*, 214 (2016) 1-7.
- [16] J. Seif, A. Descoeurdes, G. Nogay, S. Hanni, S. Nicolas, N. Holm, J. Geissbühler, A. Hessler-Wyser, M. Duchamp, R. Dunin-Borkowski, M. Ledinsky, S. de Wolf and C. Ballif, "Strategies for Doped Nanocrystalline Silicon Integration in Silicon Heterojunction Solar Cells", *IEEE Journal of Photovoltaics* (2016) 1–9.
- [17] Y. Djeridane, A. Abramov and P. Roca i Cabarrocas, "Silane versus silicon tetrafluoride in the growth of microcrystalline silicon films by standard radio frequency glow discharge", *Thin Solid Films*, 515 (2007) 7451–7454.
- [18] N. Pellaton Vaucher, B. Rech, D. Fischer, S. Dubail, M. Goetz, H. Keppner, N. Wyrsh, C. Beneking, O. Hadjadj, V. Shklover and A. Shah, "Controlled nucleation of thin microcrystalline layers for the recombination junction in a-Si stacked cells", *Solar Energy Materials and Solar Cells*, 49 (1997) 27–33.
- [19] P. Pernet, M. Hengsberger, C. Hof, M. Goetz and A. Shah, "Growth of Thin  $\mu\text{c-Si:H}$  Layers for pin Solar Cells: Effect of the H<sub>2</sub>- or CO<sub>2</sub>-Plasma Treatments", *16th EC Photovoltaic Solar Energy Conference* (2000) 498–501.
- [20] J. Koh, H. Fujiwara, R. Koval, C. Wronski and R. Collins, "Real time spectroscopic ellipsometry studies of the nucleation and growth of p-type microcrystalline silicon films on amorphous silicon using B<sub>2</sub>H<sub>6</sub>, B(CH<sub>3</sub>)<sub>3</sub> and BF<sub>3</sub> dopant source gases", *Journal of Applied Physics*, 85 (1995) 4141.
- [21] T. Watahiki, T. Furuhashi, T. Matsuura, T. Shinagawa, Y. Shirayanagi, T. Morioka, T. Hayashida, Y. Yuda, S. Kano, Y. Sakai, H. Tokioka, Y. Kusakabe and H. Fuchigami, "Rear-emitter Si heterojunction solar cells with over 23% efficiency", *Applied Physics Express*, 8 (2015) 21402.
- [22] J. Kegel, H. Angermann, U. Stürzebecher, E. Conrad, M. Mews, L. Korte and B. Stegemann, "Over 20% conversion efficiency on silicon heterojunction solar cells by IPA-free substrate texturization", *Appl. Surf. Sci. (Applied Surface Science)*, 301 (2014) 56–62.
- [23] W. Kern, "The Evolution of Silicon Wafer Cleaning Technology", *Journal of The Electrochemical Society*, 137 (1990) 1887.
- [24] R. Santbergen, A. Smets and M. Zeman, "Optical model for multilayer structures with coherent, partly coherent and incoherent layers", *Optics express*, 21 (2013) A262-7.
- [25] Z. Holman, A. Descoeurdes, L. Barraud, F. Fernandez, J. Seif, S. de Wolf and C. Ballif, "Current Losses at the Front of Silicon Heterojunction Solar Cells", *IEEE Journal of Photovoltaics*, 2 (2012) 7–15.
- [26] Z. Holman, S. de Wolf and C. Ballif, "Improving metal reflectors by suppressing surface plasmon polaritons: A priori calculation of the internal reflectance of a solar cell", *Light: Science & Applications*, 2 (2013) 106.
- [27] K. Ding, U. Aeberhard, V. Smirnov, B. Holländer, F. Finger and U. Rau, "Wide Gap Microcrystalline Silicon Oxide Emitter for a-SiO<sub>x</sub>H/c-Si Heterojunction Solar Cells", *Japanese Journal of Applied Physics*, 52 (2013) 122304.
- [28] J. Sritharathikhun, H. Yamamoto, S. Miyajima, A. Yamada and M. Konagai, "Optimization of Amorphous Silicon Oxide Buffer Layer for High-Efficiency p-Type Hydrogenated Microcrystalline Silicon Oxide/n-Type

Crystalline Silicon Heterojunction Solar Cells", Japanese Journal of Applied Physics, 47 (2008) 8452–8455.

- [29] A. Aberle, "Surface passivation of crystalline silicon solar cells: A review", Progress in Photovoltaics: Research and Applications, 8 (2000) 473–487.

- [30] A. Cuevas and D. Macdonald, "Measuring and interpreting the lifetime of silicon wafers", Solar Energy, 76 (2004) 255–262.